Eur. Phys. J. A **23**, 19–31 (2005)
DOI 10.1140/epja/i2004-10071-3

THE EUROPEAN PHYSICAL JOURNAL A

Emission of unbound ^{8}Be and ^{12}C$^{*}(0_2^+)$ clusters in compound nucleus reactions

Tz. Kokalova[1,2,a], W. von Oertzen[1,2], S. Torilov[1,2], S. Thummerer[2], M. Milin[1,2,3], A. Tumino[2,4], G. de Angelis[2,5], E. Farnea[6], A. Gadea[5], D.R. Napoli[5], Th. Kröll[5], N. Marginean[5], T. Martinez[5], M. Axiotis[5], S.M. Lenzi[6], C. Ur[6], P. Papka[7], and M. Rousseau[7]

[1] Freie Universität Berlin, Fachbereich Physik, Arnimallee 14, D-14195 Berlin, Germany
[2] Hahn-Meitner-Institut Berlin, Glienicker Straße 100, D-14109 Berlin, Germany
[3] Ruđer Bošković Institute, Zagreb, Croatia
[4] INFN-Laboratori Nazionali del Sud and Università di Catania, Catania, Italy
[5] INFN-Laboratori Nazionali di Legnaro, Legnaro, Italy
[6] Dipartimento di Fisica and INFN, Padova, Italy
[7] Institut de Recherches Subatomiques, IReS, Strasbourg, France

Received: 28 April 2004 / Revised version: 10 June 2004 /
Published online: 24 November 2004 – © Società Italiana di Fisica / Springer-Verlag 2004
Communicated by J. Äystö

Abstract. We have studied the emission of light unbound clusters, ^{8}Be and ^{12}C$^{*}(0_2^+)$, in the reactions ^{18}O + ^{13}C → ^{31}Si → ^{23}Ne + ^{8}Be and ^{28}Si + ^{24}Mg → ^{52}Fe → ^{40}Ca + ^{12}C$^{*}(0_2^+)$. The γ-ray spectra obtained in coincidence with ^{8}Be and ^{12}C$^{*}(0_2^+)$ emission have been studied relative to the statistical emission of two or three α-particles. The angular-momentum–to–energy balance of the cluster emission is compared with that of multiple-α emission. The properties of the energy spectra of the binary process and the population of the residual nuclei by cluster emission are discussed. It is observed that cluster emission carries away less excitation energy on average than the sequential emission of the individual components.

PACS. 21.60.Gx Cluster models – 23.90.+w Other topics in radioactive decay and in-beam spectroscopy – 25.70.Gh Compound nucleus – 25.70.Pq Multifragment emission and correlations

1 Introduction

In nuclear structure studies the evaporation of light particles following compound nucleus formation is a decay process which is commonly used to produce residual nuclei, which can be subsequently studied via γ-ray spectroscopy. Less used is the emission of heavier charged clusters, a mechanism which is of interest for the study of properties of compound nuclei [1] and it may be able to produce nuclei in states of angular momentum and excitation energy that are not normally populated via light-particle emission [2]. Large γ-ray detector arrays like EUROBALL and GASP often make use of light charged-particle triggers to select a particular γ-decaying nucleus [3]. The detection of γ-rays in coincidence with heavier clusters is generally more difficult requiring the integration of large gas counters with close-packed germanium detector arrays like the Binary Reaction Spectrometer (BRS) [4]. As a step to the study of γ-ray decays in binary processes we have studied the γ-ray decay of compound nuclei in coincidence with cluster decay reaction products populated in excited states just above the particle threshold, and as a trigger we have used the decay into two or more α-particles.

2 Experimental set-up

The experiments discussed below have been performed at the Legnaro National Laboratory using the γ-detector array GASP, consisting of forty high-purity germanium detectors and a multiplicity filter of eighty BGO scintillators. Light charged particles have been detected by the ISIS silicon ball [5] consisting of forty ΔE-E telescopes each covering a solid angle of about 0.20 sr (which corresponds to a width of 29° in the reaction plane). Strongly correlated α-particles emitted in the decay of weakly unbound cluster states are detected in the same silicon telescopes and observed through the pile-up of signals. The identification of the decay products produced by the cluster decay relies on the former being emitted in a narrow angular cone. Such a feature is related to the relatively small decay energies

[a] e-mail: kokalova@hmi.de

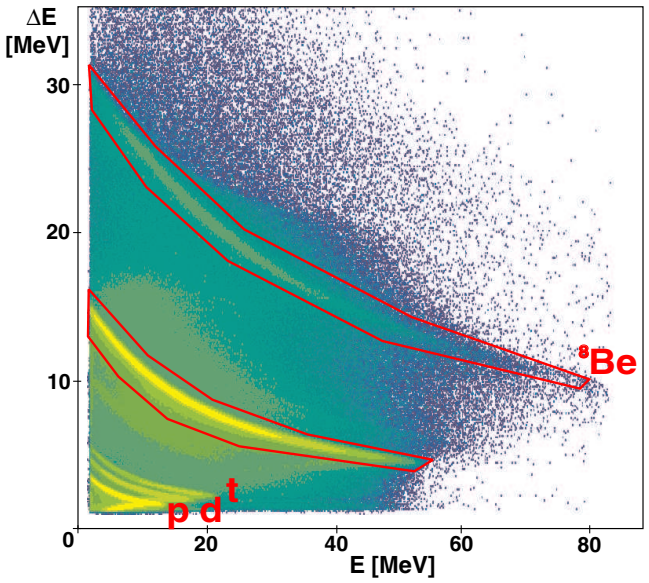

Fig. 1. An energy calibrated plot of ΔE-E signals from one of the ISIS telescopes from the first ring as obtained in the ^{18}O + ^{13}C experiment. The events representing α-particles and ^{8}Be are encircled.

of the clusters as in the case of ^{8}Be (ground state) and of the second excited state in ^{12}C$^{*}(0_2^+)$.

For the observed ^{8}Be events ($E > 30$ MeV) (see fig. 1) the decay α-particles are focused in a narrow cone (4°–6°), the axis of which lies in the direction of the original ^{8}Be events [6]. Similarly, by the instantaneous break-up of the excited 0_2^+ state in ^{12}C, three α-particles are emitted in a cone (approximately 10°–15°) within the opening angle of the individual ISIS telescopes creating triple pile-up events. In both cases (^{8}Be(0^+) and ^{12}C$^{*}(0_2^+)$), since all the spins involved are zero, the angular distribution of the emitted α-particles should be isotropic in the intrinsic frame and no correlations are expected relative to the emission axis (or the beam axis).

Here, results from two different reactions will be presented with the observation of ^{8}Be(0^+) and ^{12}C$^{*}(0_2^+)$ cluster emission:

1) ^{18}O + ^{13}C $\rightarrow$ ^{31}Si $\rightarrow$ ^{23}Ne + ^{8}Be, at an incident energy of $E_L(^{18}\mathrm{O}) = 100$ MeV, also with the sequential emission of two α-particles, intended for the spectroscopic study of Ne isotopes. In the case of ^{8}Be emission it is not possible to distinguish between the ground state, which is unbound by only 91.9 keV and the first excited 2^+ state. The latter, having a width of 1.5 MeV at an excitation energy of 3.04 MeV, has a decay cone of more than 30° (for the observed ^{8}Be events, which have $E > 30$ MeV). Due to this large maximum angle between the two α-particles coming from the decay of the 2^+ state, the efficiency for registering such events in one ISIS telescope is rather small.

2) ^{28}Si + ^{24}Mg $\rightarrow$ ^{52}Fe $\rightarrow$ ^{40}Ca + ^{12}C* or with the sequential emission of three α-particles, at an incident energy of $E_L(^{28}\mathrm{Si}) = 130$ MeV. This experiment was designed to observe the emission of ^{8}Be and the three-α channel as the main compound decays. This allows the observation of reactions involving the emission of ^{8}Be plus one α-particle, as well as of ^{12}C* in the excited 0_2^+ state at an excitation energy of 7.654 MeV, 288 keV above the three-α threshold.

2.1 The ISIS detector and multiplicities

Gamma-particle coincidence events were collected using the GASP germanium array in coincidence with the ISIS charged-particle detector [5]. This combination enables discrimination between the different reaction channels by selecting the proper number of evaporated light charged particles detected in the silicon telescopes and the corresponding γ-ray decay. Absorber foils of 12 μm thick aluminium were mounted as follows: one cylindrical along the beam axis and a second one facing the target to prevent scattered beam particles from penetrating the silicon detectors.

The total solid angle covered by the ISIS detectors is 64% of 4π sr. Due to the width of the detector frames, there are gaps of approximately 6°–7° between adjacent detectors. The kinematic conditions for the cluster decay mentioned in sect. 2 allow us to neglect the contribution from the α-particle events arising from cluster decay products entering two neighbouring detectors. In the case of ^{8}Be the events with two α's in neighbouring detectors could also originate from the excited 2^+ state.

Plotting the energy signal of the first (thin-ΔE) detector *vs.* the signal of the second (thick-E) detector, the events for each mass (m) and charge (Z) with different mZ^2 values will follow the simplified Bethe-Bloch formula (see eq. (1) and ref. [7]) and will be separated into a distinct banana-shaped distribution:

$$\frac{\mathrm{d}E}{\mathrm{d}x} \propto \frac{mZ^2}{E}\,. \qquad (1)$$

The spectra for each silicon detector were adjusted so that the particle distributions could be summed to give a total ΔE-E matrix.

The ^{8}Be and ^{12}C$^{*}(0_2^+)$ emission events are registered as multiple-hit signals in the identification plots, with two- or three times higher values than the original signals described by Bethe-Bloch curves for the single α-particles. Figure 1 shows a characteristic ΔE-E plot from an ISIS telescope, as obtained in the ^{18}O + ^{13}C experiment. The regions of "^{8}Be" and α events are marked. The separation between the light charged particles (p, d, t) is also clearly seen. For the second experiment a ΔE-E plot from all of the ISIS detectors is shown in fig. 2. The "shadow" at the left side of the picture is an electronic pile-up effect due to the high yield of protons and deuterons.

In the emission of two or three α-particles from an unbound state, each α-particle obtains, in their centre-of-mass frame, an energy of around 100 keV or less (the original binary fragment being emitted with an energy of typically 30–50 MeV). Thus, the momentum vectors of such α-particles in the laboratory frame are almost the

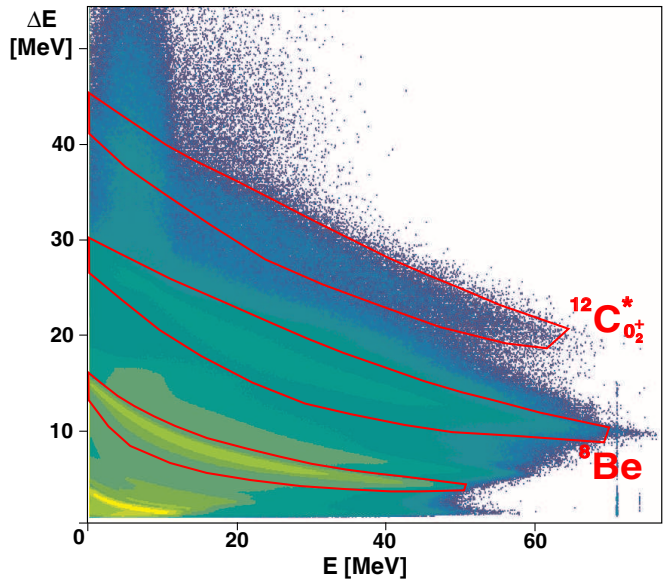

Fig. 2. An energy calibrated plot of all ΔE-E signals from the ISIS telescopes obtained in the ^{28}Si + ^{24}Mg experiment. Regions used for the identification of α-particles, ^{8}Be and ^{12}C$^{*}(0_2^+)$ are encircled.

Table 1. The α-particle event rates observed in the laboratory system for the different multiplicities ($i\alpha$, $i = 1, 2, 3, 4$) from the two experiments. The relative intrinsic event rate was obtained by *removing* the α-efficiency, $\varepsilon_i = (\varepsilon_1)^i$, where $\varepsilon_1 = 33\%$, and normalising to $N(1\alpha)$ for each reaction.

	^{18}O + ^{13}C			
	All detectors		Ring 1	
	exp.	rel.	exp.	rel.
$N(1\alpha)$	5.4×10^{7}	1.0	4.3×10^{7}	1.0
$N(2\alpha)$	4.5×10^{6}	0.25	3.6×10^{6}	0.25
$N(3\alpha)$	4.2×10^{4}	7.1×10^{-3}	3.2×10^{4}	6.8×10^{-3}
$N(4\alpha)$	9×10^{2}	4.6×10^{-4}	6.9×10^{2}	4.5×10^{-4}
^{8}Be	1.42×10^{6}		1.38×10^{6}	
	^{28}Si + ^{24}Mg			
	All detectors		Ring 1	
	exp.	rel.	exp.	rel.
$N(1\alpha)$	6.9×10^{7}	1.0	3.6×10^{7}	1.0
$N(2\alpha)$	2.9×10^{7}	1.27	1.5×10^{7}	1.26
$N(3\alpha)$	3.2×10^{6}	0.43	1.7×10^{6}	0.43
$N(4\alpha)$	7.5×10^{4}	3.0×10^{-2}	4.0×10^{4}	3.1×10^{-2}
^{12}C	1.03×10^{6}		9.83×10^{5}	

same. As a consequence, the multiple-hit signals associated with the detection of such strongly correlated decay products in the same telescope lie on an event line which corresponds to a rescaling of the ΔE and E signals, *i.e.* having a functional dependence described again by the Bethe-Bloch formula.

For both reactions the observed multiplicities and the relative event rates are given in table 1. An α-detection efficiency, ε_1, of 33% was extracted from the data by examining the relative strengths of transitions in the same nucleus in the two-α channel in two different γ-γ matrices, those gated by one or two α-particles, respectively. From these results we can evaluate the multiple-hit probabilities, which are discussed in the next section. Note that the maxima in the event rates for the ^{18}O + ^{13}C and ^{28}Si + ^{24}Mg experiments lie at multiplicities of one and two α-particles, respectively.

The majority of the two or three α-particle events, 97% and 96%, respectively (see table 1) due to cluster decay are observed in the first ring of the ISIS detector system. The first ring consists of six silicon telescopes at an average angle of 34°. Taking only the events from the first ring gives us the opportunity to compare the cluster emission and the sequential α-particle emission under the same kinematical conditions.

The original strength of the emission sources for the ^{8}Be and ^{12}C* from the compound nucleus have to be calculated as described in the next sections.

2.2 Multiple-hit probabilities

For a quantitative evaluation of the cluster decay, the probability to have multiple-hit events due to higher multiplicities entering into one ΔE-E telescope must be discussed. The ISIS spectrometer was built to have a multiple-hit event rate of less than 2% even for high multiplicities [8], though for a reaction covering a solid angle of 4π sr.

For the data obtained in the ^{18}O + ^{13}C and ^{28}Si + ^{24}Mg experiments the event rate for two or three α-particles registered in the same detector compared to the two or three α-particles in different detectors is evaluated as follows. In the reaction the compound nucleus emits α-particles with multiplicity M. For N_D detectors, each covering a fraction $\varepsilon^{\star}$ of the solid angle, the probability of detecting F(Fold) α-particles of multiplicity (M) will be [9]:

$$P(F,M) = \binom{M}{F} (N_D\varepsilon^{\star})^F (1 - N_D\varepsilon^{\star})^{M-F}. \qquad (2)$$

Here, $\binom{M}{F}$ is the binomial coefficient and $N_D\varepsilon^{\star}$ is the total efficiency. This expression is valid for the centre-of-mass system and, in transforming it to be applicable in the laboratory system, the geometrical efficiency ($\varepsilon^{\star}$) has to be multiplied by a kinematical compression factor, given by the Jacobian (J). The Jacobian is a function of the reaction angle and the Q-value which transforms the "phase space" of the centre-of-mass system into the "phase space" of the laboratory system. For the latter we define the detection efficiency, ε_i (where $i = 1$ for one α; $i = 8$ for ^{8}Be and $i = 12$ for ^{12}C), as

$$\varepsilon_i = \varepsilon^{\star} J_i \qquad (3)$$

and this depends on the angle and on the reaction. We use average values of the Jacobians for angles representing the centre of the detectors in the first ring and

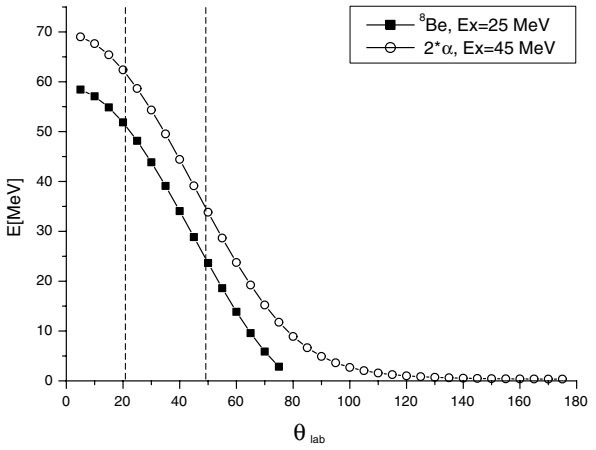

Fig. 3. Calculated kinematical plots for the angular variation of the energy of two α-particles and of ^{8}Be. Dashed lines indicate the angular width of the first ring of ISIS detectors. Q-values are chosen to have an excitation energy (E_x) in the residual nuclei, as indicated.

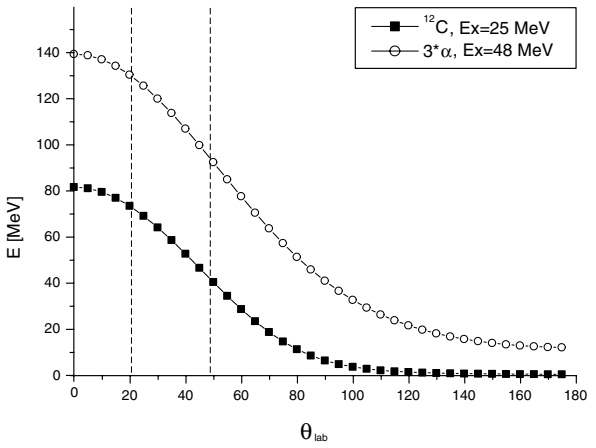

Fig. 4. Calculated kinematical plots for the angular variation of the energy of three α's and of ^{12}C$^*(0_2^+)$. Dashed lines indicate the angular width of the first ring of ISIS detectors (see also fig. 3).

Q-values giving the maxima in the energy spectra. The corresponding Jacobians are

$$^{18}\mathrm{O} + {}^{13}\mathrm{C} : J_1 = 1.9 \text{ and } J_8 = 2.7,$$
$$^{28}\mathrm{Si} + {}^{24}\mathrm{Mg} : J_1 = 2.1 \text{ and } J_{12} = 3.0. \quad (4)$$

The kinematical variations for the typical Q-values are shown in figs. 3 and 4 for the two reactions, respectively. Variations due to the excitation energy are not considered at this stage, but see the discussion in sect. 3.1.

We keep the expression (eq. (2)), but replace $\varepsilon^\star$ with ε_i, indicating that these factors are included. Note that the geometrical efficiency $\varepsilon^\star$ of the six telescopes of the first ring is ~ 1.2 sr. This value is only needed if we want to calculate the absolute rate. *In the following, only ratios are used.*

In the case $M = F = 2$ the total probability of detecting two out of two α-particles in all detectors is

$$P(2,2) = (N_D\varepsilon_1)^2. \quad (5)$$

The probability of detecting two out of two α-particles in two separate detectors is P_{sh}(single hit) is

$$P_{\mathrm{sh}}(2,2) = N_D(N_D-1)\varepsilon_1^2\,. \quad (6)$$

Accordingly, the probability of *double hits* in a single detector will be given by the difference

$$P_{\mathrm{dh}}(2,2) = P(2,2) - P_{\mathrm{sh}}(2,2) = N_D\varepsilon_1^2\,. \quad (7)$$

Thus, the ratio of chance double hits observed as pile-up signals in one detector compared to registering the two α-particles in separate detectors (for an equal and isotropic probability for emitting a single α-particle) is

$$\frac{P_{\mathrm{dh}}(2,2)}{P_{\mathrm{sh}}(2,2)} = \frac{1}{N_D-1}\,, \quad (8)$$

which is independent of the solid angle $\varepsilon^\star$.

The probability of detecting two α-particles coming from ^{8}Be in a single detector is

$$P(^8\mathrm{Be}) = N_D\varepsilon_8\,. \quad (9)$$

Thus, one can build the ratio of the probability of detecting ^{8}Be to the probability of detecting two out of two α-particles ($F = 2$) in different detectors (using eq. (2)),

$$\frac{P(^8\mathrm{Be})}{P_{\mathrm{sh}}(2,2)} = \frac{\varepsilon_8}{(N_D-1)\varepsilon_1^2}\,. \quad (10)$$

The same considerations can be made for the registration of three α-particles and ^{12}C*. In this case for $F = M = 3$ the total probability for detecting three α-particles in *all* detectors is (using eq. (2))

$$P(3,3) = (N_D\varepsilon_1)^3. \quad (11)$$

In the case of detecting three α-particles in *different* detectors, the probability will be

$$P_{\mathrm{sh}}(3,3) = N_D(N_D-1)(N_D-2)\varepsilon_1^3\,. \quad (12)$$

Building the difference from these two equations, one can obtain the probability of *triple hits* in one detector:

$$P_{\mathrm{trh}}(3,3) = P(3,3) - P_{\mathrm{sh}}(3,3) = N_D(3N_D-2)\varepsilon_1^3\,. \quad (13)$$

Thus, the ratio of chance triple hits observed as pile-up signals in one detector compared to the three α-particles registered in separate detectors ($F = 3$) (for an equal and isotropic probability for emitting a single α-particle) is

$$\frac{P_{\mathrm{trh}}(3,3)}{P_{\mathrm{sh}}(3,3)} = \frac{3N_D-2}{(N_D-1)(N_D-2)}\,. \quad (14)$$

For the detection of ^{12}C*, since the emitted particles are registered in *one* telescope, the probability is

$$P(^{12}\mathrm{C}^*) = N_D\varepsilon_{12}\,. \quad (15)$$

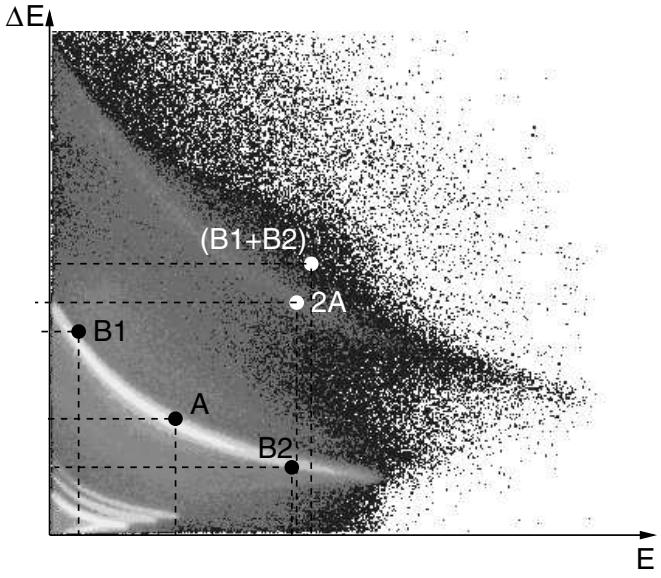

Fig. 5. Schematic illustration of the deviation of the random double-hit events from the event line of the coincident α-particles from the ^{8}Be emission. Two ΔE-E signals for different energies (case B1, B2) and for equal energies (case A) are indicated. The events represent the data of fig. 1.

Using these equations, the ratio of the probability of detecting ^{12}C* to the probability of detecting three out of three α-particles ($F = 3$) in different detectors can be built:

$$\frac{P(^{12}\mathrm{C}^{*})}{P_{\mathrm{sh}}(3,3)} = \frac{\varepsilon_{12}}{(3N_D-2)\varepsilon_1^3}\,. \tag{16}$$

For the comparison of the charged-particle spectra and their ratios in sect. 3.1, the Jacobians for the emission of the first and second α-particles have been assumed to be equal, which is reasonable for the purpose of our study. Also, the variation of the Jacobian with energy is assumed to be similar for the different reactions, involving α-particles, ^{8}Be and ^{12}C ejectiles. For these considerations the kinematical curves are shown in figs. 3 and 4 for the two reactions.

In this discussion an average value for the Jacobians, $(J(E_\alpha))$, which depends on E_α and the emission angle is assumed; E_α represents the maximum of the energy spectra and varies only slightly from the first emission step up to the third. We can also conclude (see table 1) that the contributions from higher multiplicities to lower folds, according to eq. (2) (*e.g.* of $M = 3, 4\ldots$ to $F = 2$ or $M = 4, 5\ldots$ to $F = 3$) for the pile-up coincidences can be neglected.

Now the ΔE-E spectra of multiple-hit events must be considered. For $E_{\alpha_1} = E_{\alpha_2}$ we have already stated that the events will follow the Bethe-Bloch dependence (case A in fig. 5). The contribution to coincidences in the same telescope coming from evaporated α-particles with different energies will be distributed over a wider range in the pile-up region in the ΔE-E plots. Indeed, we observe a deviation for the ^{8}Be events from the Bethe-Bloch function in fig. 1 (repeated schematically in fig. 5). For $E_{\alpha_1} \neq E_{\alpha_2}$ (case B1 + B2 in fig. 5), the total energy ($E = E_{\alpha_1} + E_{\alpha_2}$) distribution will not follow the Bethe-Bloch dependence because of the non-linear dependence ($1/E$) of the ΔE signal. This deviation can be clearly seen by constructing the multiple-hit events using two very different values of the energies for the two detected α-particles. In the case of an uncorrelated emission, where the energies of the two α-particles are very different (B1 and B2 in fig. 5), we have E (multiple hit) = B1+B2. This implies that chance coincidences start to deviate towards higher ΔE values with respect to the rescaled Bethe-Bloch line of the ^{8}Be. A similar effect is expected for the ^{12}C* line, although here the probability of chance coincidences for three α-particles contributing to the cluster decay event line is very small (see fig. 2 and sect. 3.1).

In the case of ^{8}Be and ^{12}C* emission the relative energies of the emitted α-particles in the centre-of-mass system are very small compared to the emission energy of the cluster. Therefore, the final energies of the α-particles originating from cluster decay, $E_{\alpha_i} (i = 1, 2, 3)$, are almost the same and the corresponding energy spectrum from the piled-up events represents the energy of the original cluster, because we have:

$$\begin{aligned} &E_{\alpha_1} \approx E_{\alpha_2} \approx E_{\alpha_3}\,, \\ &E_{\mathrm{cluster}} = \sum_i E_{\alpha_i}\,. \end{aligned} \tag{17}$$

In these events there is no time delay (except for the compound nucleus lifetime) between the individual α-particles.

The decay of ^{12}C$^{*}(0_2^+)$ is known to proceed predominantly via the $^{8}\mathrm{Be} + \alpha$ channel. The lifetime of $^{8}\mathrm{Be} \rightarrow \alpha + \alpha$ decay is approximately 10^{-16} s and for the detection of the three-α pile-up this time delay is of no relevance. For the triple α-events in addition the decay of higher excited states of, *e.g.* ^{12}C$^{*}(0_3^+,\ 10.3\,\mathrm{MeV})$, is expected to contribute.

According to eq. (17), we may tentatively take the rescaled energy spectra (see sect. 3.1) corresponding to the emission of two or three α-particles (Fold = 2 or 3) to enable a comparison between the multiple-hit events and the ^{8}Be or ^{12}C* spectra (see figs. 8 and 9). Such comparisons hold true only around the maxima (as a function of energy) of the distributions for Fold = 2 or 3. In addition to the true ^{8}Be and ^{12}C* events, there may be random counts from (sequential) compound nucleus emissions from *different reactions*, which can produce coincidences with events of two and three α-particles with the same energies, which may not deviate from the rescaled Bethe-Bloch line to larger ΔE values. In order to assess these contributions, a simple formula for random coincidences, N^{random}, can be used

$$N_{2\alpha}^{\mathrm{random}}(E) = N_\alpha^2(E_\alpha)\Delta\tau. \tag{18}$$

The counting rates, N_α, can be taken from the running time and the total number of events in the α-particle curve. The full range of the time coincidence window is

1 μs, but this was redefined in software during the off-line analysis by placing a 90 ns gate around the prompt time peak. (N.B.: The integration time in the electronic amplifier converting the signals is $\sim$ several μs.) Therefore, $\Delta\tau$, is the 90 ns time window during which random coincidences could occur. Thus, the calculated value for $N_{2\alpha}^{\rm random}$ is less than 0.03% and can be neglected. This means that each event contains multiple-hit coincidences from just one reaction.

3 Results and discussion of cluster emission as a statistical process

3.1 Discussion of the charged-particle energy spectra

Using the calibrated ΔE-E signals, we have compared the total energy spectra of the reconstructed cluster emissions with those of the expected multiple-hit events due to the detection of two or more evaporated α-particles.

We first consider the case of ^{18}O + ^{13}C. A quantitative evaluation of the expected double-hit event rate can be obtained by examining the two-α yields in pairs of detectors in the first ring of the ISIS array. The six detectors are arranged clockwise as follows: #1 ($\phi = 0°$), #5 ($\phi = 297°$), #3 ($\phi = 238°$), #0 ($\phi = 180°$), #4 ($\phi = 117°$), #2 ($\phi = 58°$) (see fig. 6). Examining the two-α event rates in pairs of ISIS detectors in the first ring, as a function of angle (see fig. 7), the highest coincidence rates are in opposite detectors, demonstrating that the sequentially emitted α-particles are preferentially emitted in opposite directions. Furthermore, extrapolating these distributions it is possible to extract an estimate of the relative double-hit event rate, *i.e.* two α-particles in one detector. In addition, the measured ^{8}Be intensities are also shown in fig. 7. There is a clear dominance (by a factor of 6–8) of the "real" ^{8}Be events over the uncorrelated double hits for the registered pile-up events.

For the comparison of the ^{8}Be or ^{12}C* emission with the multiple-hit events, an energy spectrum is built by adding the events (*e.g.* $\sum_i N(E_{\alpha_i})$ $(i = 1, 2, 3)$) of two (three) α-particles, $F = 2$ ($F = 3$), detected in two (three) different detectors from the first ring, so that the kinematical conditions are the same for all detectors. The event rate is rescaled by division by a factor of two (three) and the energy scale expanded by a factor of two (three); see figs. 8 and 9. For comparison with the ^{8}Be spectra ($F = 1$), the difference in the kinematic behaviour of the reaction ^{13}C(^{18}O, ^{8}Be)^{23}Ne and the reaction ^{13}C(^{18}O, ^{4}He)^{27}Mg has to be considered. For this purpose we have shown, for the two cases, the energy variation with angle in fig. 3. For these calculations, the Q-values have been fixed to correspond to the typical excitation energy of the residual nucleus as indicated in the figs. 3 and 4. The angular width of the first ring of ISIS telescopes is indicated by dashed lines; the energy variations are very similar in this region.

For the two-α-particle events from ^{8}Be it is necessary to take account of the Jacobians, which enter into the efficiency of the detectors in the laboratory system. The values of the Jacobians for both reactions are given in sect. 2.2 (see eq. (4)).

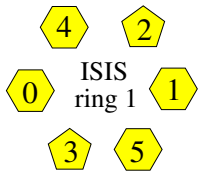

Fig. 6. First ring of the ISIS detector array comprising six detectors. The numbering is used in fig. 7 with the notation $[i, j]$.

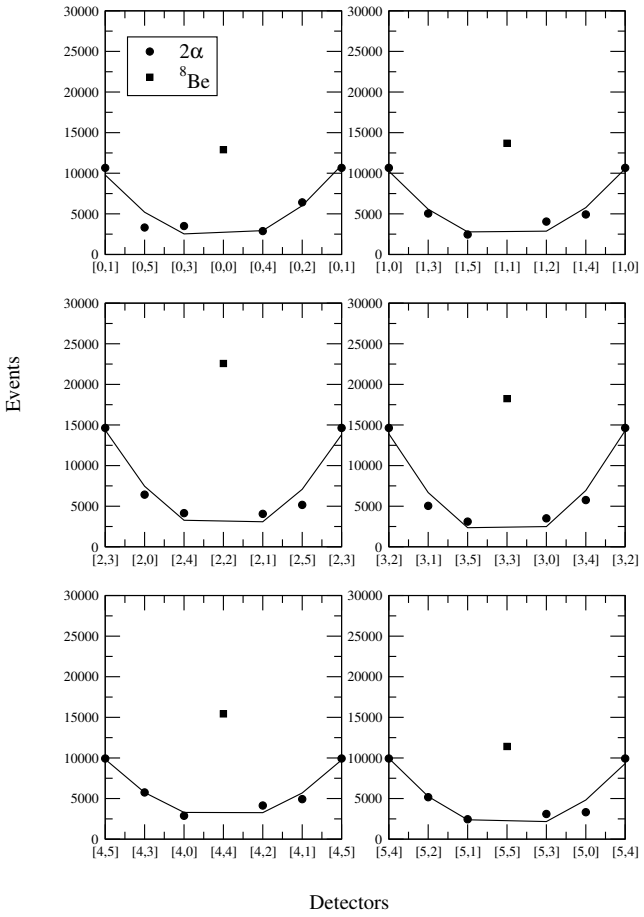

Fig. 7. Event distributions in the first ISIS ring for two α-particles (filled circles) registered in different pairs of detectors and ^{8}Be (filled squares). The combinations of two detectors i, j according to fig. 6 are indicated on the horizontal axis as $[i, j]$, for all $i = 0, \ldots 5$. The solid line is to guide the eye. Note that the far right and the far left points on any given panel are duplicates, shown twice for clarity.

For the comparison of the observed energy spectra, taking into account the formulæ for the probabilities (see eq. (10)) in the case of the emission of two α-particles, we obtain the ratio

$$\frac{N^{*}_{^{8}\mathrm{Be}}}{N^{*}_{2\alpha}} = \frac{N_{^{8}\mathrm{Be}}}{N_{2\alpha}} \frac{1}{(N_D - 1)} \frac{J_8}{\varepsilon^{\star} J_1^2}\,, \qquad (19)$$

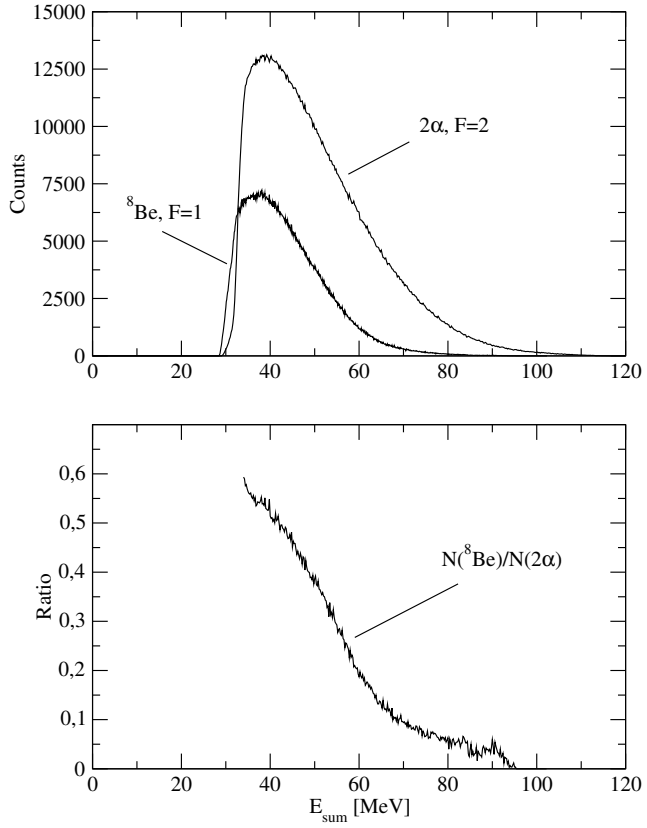

Fig. 8. Upper panel: Total energy spectra ($E_{\rm sum} = \Delta E + E$) as observed with the ISIS charged-particle detector system for the emission of single α's in two detectors (Fold = 2), and of ^{8}Be, in the reaction ^{18}O + ^{13}C. Note that the two-α curve is constructed from events with $F = 2$, but with the energy scale multiplied by a factor of two to enable a comparison between the ^{8}Be and $F = 2$ distributions. The vertical scale has been adjusted to show qualitatively the differences. Lower panel: the ratio between these two experimental curves.

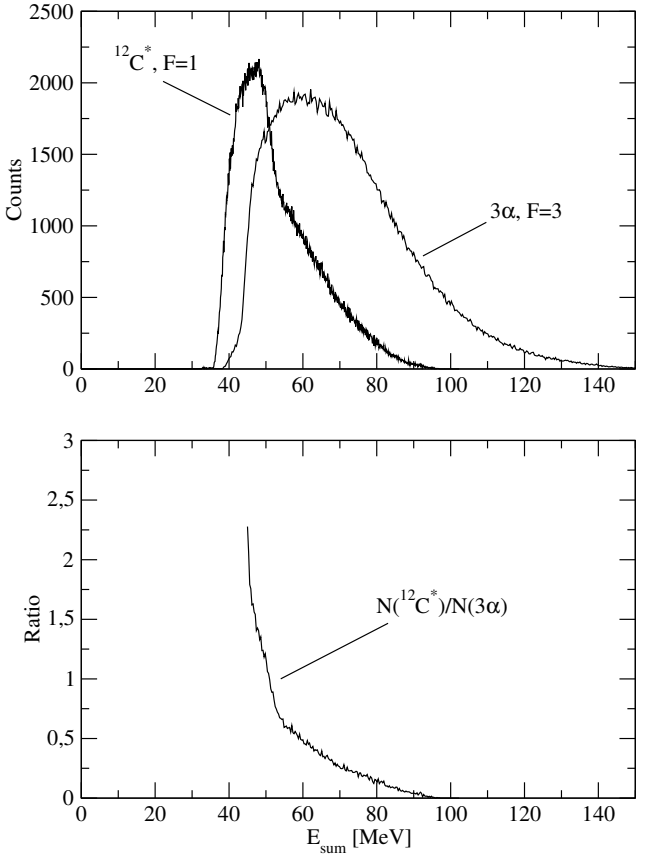

Fig. 9. Upper panel: Total energy spectra ($\Delta E + E$ signals) as observed with the ISIS charged-particle detector system for the emission of three single α's ($F = 3$), and of ^{12}C$^*(0_2^+)$ in the reaction ^{28}Si + ^{24}Mg. Note that the three-α curve is constructed from events with $F = 3$, but with the energy scale multiplied by a factor of three to enable a comparison between the ^{12}C$^*(0_2^+)$ and $F = 3$ distributions. The vertical scale has been adjusted to show qualitatively the differences. Lower panel: the ratio between these two curves.

where $N^*_{^8\mathrm{Be}}$ and $N^*_{2\alpha}$ are the experimentally observed counting rates for ^{8}Be and two α's respectively, $N_{^8\mathrm{Be}}$ and $N_{2\alpha}$ are the original compound nucleus emission rates, and J_8 and J_1 are the corresponding Jacobians. For the case of three α-particles, using eq. (16) we have the ratio

$$\frac{N^*_{^{12}\mathrm{C}^*}}{N^*_{3\alpha}} = \frac{N_{^{12}\mathrm{C}^*}}{N_{3\alpha}} \frac{1}{(3N_D - 2)} \frac{J_{12}}{\varepsilon^{\star 2} J_1^3}\,, \qquad (20)$$

where $N^*_{^{12}\mathrm{C}^*}$ and $N^*_{3\alpha}$ are the experimentally observed counting rates for ^{12}C and three α's respectively, $N_{^{12}\mathrm{C}^*}$ and $N_{3\alpha}$ are the original compound nucleus emission rates, and J_{12} and J_1 are the corresponding Jacobians.

The Jacobians, J_1 and J_8, for the centre ($\theta = 34°$) of the telescopes are unequal (see sect. 2.2) and for the same centre-of-mass emission probability the observed ratio of $\frac{N^*_{^8\mathrm{Be}}}{N^*_{2\alpha}}$ contains the factor $\frac{J_8}{\varepsilon^\star J_1^2} = \frac{0.75}{\varepsilon^\star}$. This means that compared to the centre-of-mass detection probability the measured $N(^8\mathrm{Be})$ is enhanced by a factor of ≈ 2, relative to $N(2\alpha)$.

In the following we compare the energy spectra of the emitted clusters with the expected energy of the multiple-hit events. The latter is not taken just as a rescaled single α-spectrum ($E_{\rm dh} = 2E_{1\alpha}$) but the intensities of $N(E_{\alpha_1})$ and $N(E_{\alpha_2})$ are added, and the energy is then rescaled by a factor of two. This takes into account that a larger (than average) E_{α_1} is typically followed by a smaller E_{α_2} value. The same procedure is followed for triple hits and ^{12}C*.

From the considerations in sect. 2.2, we would have expected for only $F = 2$, $M = 2$ events in the ^{8}Be line a constant value, as a function of the energy, of 0.2 ($= N_{\rm dh}(2,2)/N_{\rm sh}(2,2)$). We observe a higher value at the energy maxima and a much smaller value (0.05) at higher energies. This indicates that the ^{8}Be are mainly observed at lower energies whereas at higher energies the lower values can be explained as being due to the non-isotropic emission in the sequential process (see fig. 7).

The same kind of calculation for $M = 3$ and $F = 3$ gives, for the ratio (see eq. (14)) of the number of pure

triple hits from sequentially emitted α-particles to those of three α-particles in different detectors, a constant ratio, as a function of the energy, of 0.8 $(= 18 - 2/((6-1)(6-2)))$. This value is rather large because of the small number of detectors, but again, a higher value was observed at low energies and (see fig. 9), and at higher energies the measured ratio becomes very small. Once more this is explained by the fact that the three sequential α-particles do not have an isotropic angular distribution.

The considerations for the ^{24}Mg(^{28}Si, ^{12}C*)^{40}Ca and ^{24}Mg(^{28}Si, α)^{48}Cr reactions are obtained using the information from fig. 4. In this case the ratio $\frac{N^*_{^{12}\mathrm{C}^*}}{N^*_{3\alpha}}$ contains the factor $\frac{J_{12}}{\varepsilon^\star J_1^3} = \frac{2.92}{(\varepsilon^\star)^2}$. Thus, in the laboratory frame this enhances the observation of ^{12}C* relative to 3α $(F = 3)$ emission by a factor of ≈ 27, giving the proper ratio in the centre-of-mass frame of the emitting compound nucleus.

Note that in figs. 8 and 9 (upper panels) parts of the energy spectra are missing. This low-energy cut-off arises because of the minimum energy needed by the charged particles to penetrate the absorber foils and the ΔE detector and to be registered in the E detector. For ISIS this corresponds to 14.9 MeV for α-particles and to 3.7 MeV for protons. These values were used for the energy calibration of the silicon detectors.

The variation of the observed ratios from the predicted constant values (eqs. (8) and (14)) may occur for three reasons:

i) dominance of the true ^{8}Be or ^{12}C* emission;

ii) difference in the energy spectrum due to the emission process and;

iii) differences in the Jacobians (energy variations due to the kinematics, as previously discussed, are the same (see figs. 3 and 4)), though, since we are comparing data from the same ring (same angle), these are dependent only on the energy of the emitted fragment (α, ^{8}Be or ^{12}C*). However, these variations partially cancel out in the ratios. As found in the above analysis, the ratio of $N_{^8\mathrm{Be}}$ to $N_{2\alpha}$ is not constant as a function of energy which could be caused by the variation of the Jacobians as a function of energy. However, fig. 3 actually illustrates that the derivative of the energy (the energy variation) with respect to the angle, θ, is almost the same, in the region of interest, for ^{8}Be and for single α-particle emission. Similarly, the variation of the Jacobians with energy does not differ significantly between the two cases. The same statements hold for the comparison of three α- and ^{12}C*-events (fig. 4). As shown in figs. 8 and 9, the spectra have different shapes and maxima.

In both cases, for ^{8}Be and for ^{12}C* emission (see figs. 8 and 9, lower parts), we observe a rise towards small energies. There we will localise the dominant contribution of the cluster emission. Later it will be shown that these facts are consistent with the observation (discussed in more details in subsect. 3.3), that after ^{8}Be and ^{12}C* emission a large increase in the subsequent particle decay probability of the residual nucleus occurs (typically another neutron, proton or an α-particle). The residual nucleus is populated at much higher excitation energies for the cluster emission due to a much smaller energy of the emitted fragments, even though the *total Q-value is the same as for sequential α emission.*

3.2 Energy–to–angular-momentum balance

By looking at the energy–to–angular-momentum balance of the sequential emission processes *vs.* binary reactions, the differences observed in the population of the final states in the residual nuclei (^{23}Ne and ^{40}Ca) and the probability of a subsequent decay (because of a higher residual excitation energy) can be discussed further. The first step is to consider the angular momenta carried by, for example, two α-particles or a ^{8}Be cluster. The formula for the angular momentum, L_x, of a fragment, x, for a given kinetic energy, E_x, is given by

$$L_x = kR\sqrt{1 - \frac{E_\mathrm{b}}{E_\mathrm{CM} + Q - E_x}}\,, \tag{21}$$

where E_CM is the energy in the centre-of-mass system, R the radius and E_b the Coulomb barrier energy. The wave number, k, is given by the momentum divided by $\hbar$ (as used in eq. (22)). The α-particle has mass, m_α, and an average energy, E_α. If the larger cluster consists of two α-particles, the total mass is $2m_\alpha$, and if the kinetic energy of the cluster is twice the energy of a single α-particle emitted in the sequential process, there is no difference in the energy–to–angular-momentum balance of the reaction according to

$$k(^8\mathrm{Be}) = \frac{\sqrt{4m_\alpha 2E_\alpha}}{\hbar} = 2k_\alpha\,. \tag{22}$$

The origin of the difference in the population of the residual nucleus in a sequential, compared to a one-step evaporation process (for the same emitted mass), must be found in the emission process itself. There are two potential origins for the difference:

a) less angular momentum is carried away in the one-step process (cluster emission), because the geometry of the binary nuclear system is deformed and the emission occurs more like in a sticking situation, as in fission;

b) in the sequential process, because of the dependence on the level densities (which enter two or three times for two or three α-particles, respectively) the emission of more total energy is emphasised, relative to a one-step emission process of the same mass and charge. The latter aspect is discussed below in sect. 3.3. Figure 10 summarises the situation for the ^{18}O + ^{13}C reaction.

3.3 Gamma-ray coincidence spectra for different fragment emissions

We are interested in the angular momentum and the energy carried in the binary processes. The first step is to look into the relevant γ-ray spectra which belong to a given residual nucleus and a given charged-particle trigger.

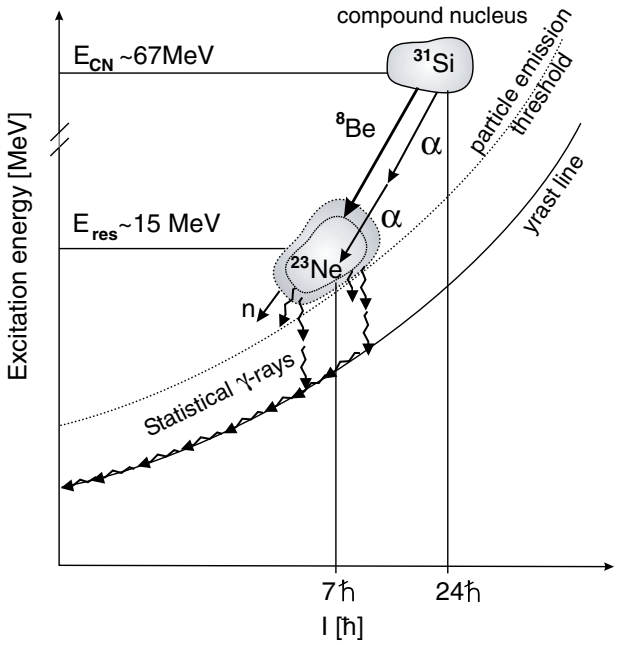

Fig. 10. Diagram of the excitation energy of the compound nucleus, *vs.* spin, I, populated in the ^{18}O + ^{13}C reaction. The scheme shows the decay of the compound nucleus via particle and γ-ray emission.

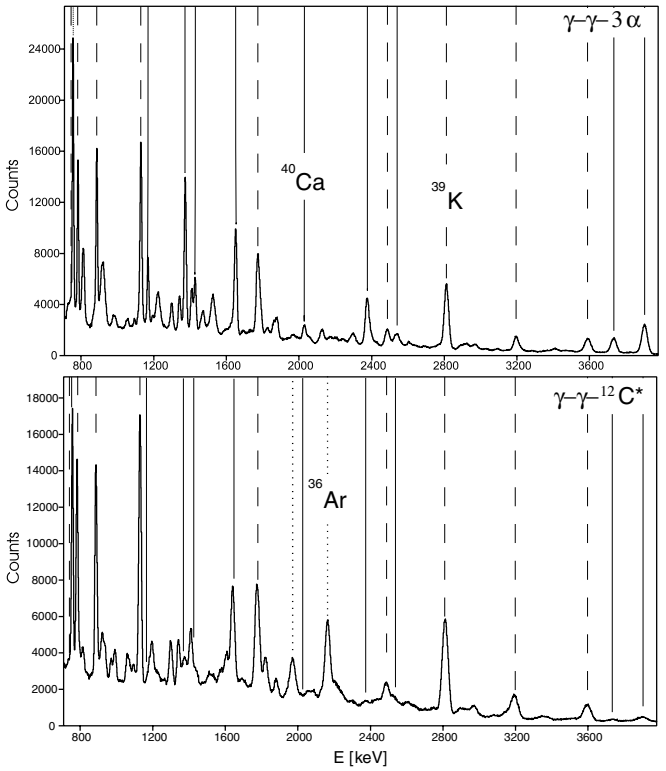

Fig. 11. Gamma-ray spectra from the ^{28}Si + ^{24}Mg reaction gated by different charged-particle triggers. The observed γ-ray transitions from different nuclei are marked as follows: solid line ^{40}Ca; dashed line ^{39}K and dotted line ^{36}Ar. Upper panel: Doppler-corrected γ-ray spectrum gated by the three-α channel. Lower panel: Doppler-corrected γ-ray spectrum gated by the ^{12}C*(0_2^+) channel; note the large contribution from ^{36}Ar in the lower panel.

In the off-line analysis the different reaction channels were selected by requiring that only the events corresponding to the detection of the proper number of α-particles (or protons) in the ΔE-E silicon telescopes were incremented into symmetrised E_γ-E_γ matrices. Generally, there are still many reaction channels due to subsequent decays (of α's, protons, neutrons) within a charged-particle ISIS trigger and additional γ-ray gates are needed to identify one residual nucleus uniquely.

For the reaction ^{18}O + ^{13}C we have just two possible triggers —two α-particles and ^{8}Be emission, giving mainly spectra of ^{21}Ne and ^{22}Ne. For the reaction ^{28}Si + ^{24}Mg the γ-ray spectra for ^{40}Ca can be obtained with three different charged-particle triggers:

a) three α-particles,
b) ^{8}Be + α-particle emission, and
c) ^{12}C*(0_2^+) emission.

Information on the emission mechanism for the ^{12}C*(0_2^+) channel is obtained via the γ-ray analysis of the ^{24}Mg(^{28}Si, ^{12}C*)^{40}Ca reaction. The relatively high velocity of the compound nucleus (CN) and the larger mass of the emitted fragments mean that the γ-ray spectra must be Doppler-corrected. A satisfactory Doppler-shift correction was obtained, resulting in an energy resolution of about 10 keV FWHM at 1000 keV. This was performed by taking the energy and angles of the particles registered in ISIS and reconstructing the trajectory of the compound residue. First the ^{28}Si + ^{24}Mg reaction will be discussed, where both ^{8}Be and ^{12}C* emission was observed. The detailed spectroscopic results from this study of the dominant residual nucleus ^{40}Ca are given in ref. [10]. Of particular interest here are the differences which are observed in the three various charged-particle triggers leading to ^{40}Ca as well as to ^{39}K after a subsequent proton emission. The results for the γ-ray projections with two different charged-particle triggers are shown in fig. 11.

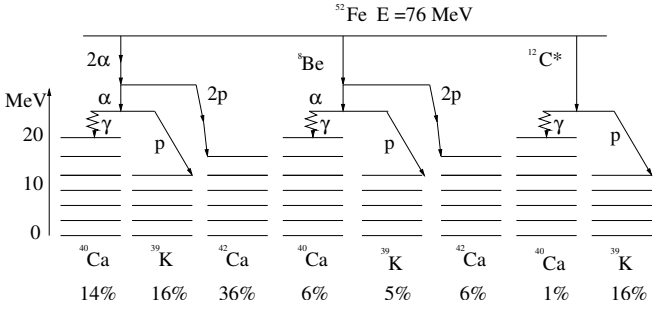

Fig. 12. Relative intensity fractions for γ-ray transitions in residual nuclei gated by three different charged-particle triggers: a) three α, b) ^{8}Be + α and c) ^{12}C*(0_2^+) from the ^{28}Si + ^{24}Mg reaction.

As stated before, a pronounced difference in the excitation energy of the residual nucleus for the emission of clusters compared to the sequential processes has been

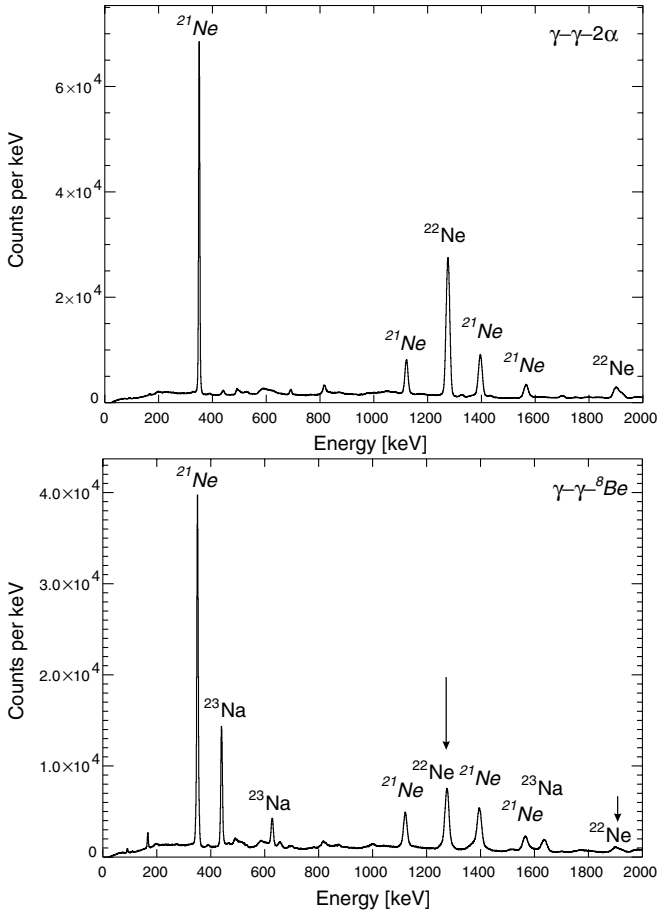

Fig. 13. Gamma-ray spectra from the $^{18}O + {}^{13}C$ reaction gated by different charged-particle triggers. Upper panel: Doppler-corrected γ-spectrum gated by the two-α channel. Lower panel: Doppler-corrected γ-ray spectrum gated by the ^{8}Be channel. The peaks corresponding to ^{23}Na are due to the emission of ^{6}Li and ^{7}Li, located within the ^{8}Be gate.

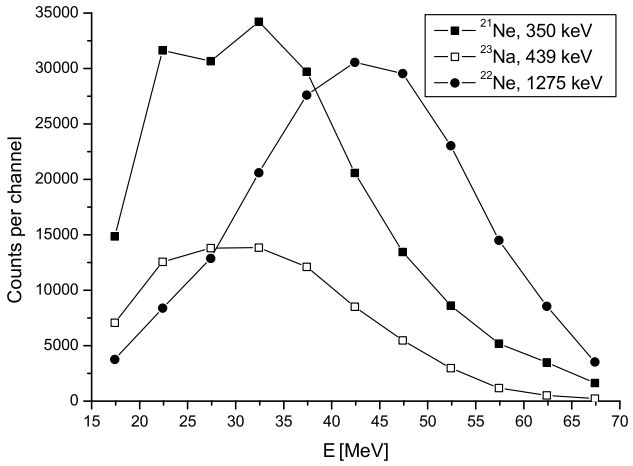

Fig. 14. Distribution of the populations of the ground-state transitions in ^{21}Ne (350 keV), ^{22}Ne (1274 keV) and ^{23}Na (439 keV) for different energies, E (*i.e.* the energies from the thick E detectors of ISIS), of the coincident two α-particles detected in the same detector (*i.e.* ^{8}Be). Note that the error bars are of the same size as the symbols or smaller.

observed for the γ-ray spectra. The relative yields are given in fig. 12 for the three different decay chains: a) three α, b) $^{8}\mathrm{Be} + \alpha$ and c) $^{12}\mathrm{C}^{*}(0_2^{+})$. By inspecting the gated spectra, one can see that the relative and absolute intensities of the lowest-lying γ-ray transitions in ^{40}Ca and ^{39}K (the latter being indicative of subsequent proton emission) are differently populated. This is due to differences in the excitation energy and angular momentum in the residual nucleus, ^{40}Ca. A more detailed view of the various channels is obtained by extracting, from the particle-γ coincidences, the relative strength observed in each channel. The data are compiled in fig. 12.

We have obtained the following results:

i) After the emission of two α's the two-p emission competes with approximately equal strength with the emission of a third α-particle (36% to [14% + 16%]).

ii) The ($^{8}\mathrm{Be} + \alpha$) emission is $\approx 1/3$ of the three-α emission ([6% + 5%] to [14% + 16%]).

iii) Finally, the $^{12}\mathrm{C}^{*}$ emission with ^{40}Ca as the residual nucleus is 1/14 of the three-α emission and the subsequent proton decay into ^{39}K has increased by a factor of 16 due to the higher residual excitation energy.

In both reactions, as already anticipated in section 3.1 and as previously observed for the ^{8}Be emission [11–13], the binary cluster channel carries less energy and less angular momentum from the residual nucleus than the sequential α-particle emission. Therefore, subsequent neutron, proton and/or α-particle evaporation becomes more conspicuous. For the $^{12}\mathrm{C}^{*}$ emission the residual nucleus has enough energy even for the subsequent emission of $2p + 2n$ or an α-particle, which leads to ^{36}Ar and some of the ^{40}Ca lines have almost disappeared in the lower panel of fig. 11.

Similarly, for the $^{13}\mathrm{C} + {}^{18}\mathrm{O}$ reaction, the strengths of the subsequent neutron decays have been compared following the emission of two α's and a ^{8}Be, namely, the subsequent $1n$ and $2n$ channels, populating the residual nuclei ^{22}Ne and ^{21}Ne, respectively. As can be seen from fig. 13, where the γ-ray coincidence spectra with a ^{8}Be gate is shown, the subsequent neutron emission is enhanced. Comparing the γ-ray spectra triggered on two α-particles (Fold = 2) the ratio between the population of ^{22}Ne (transition from the first excited state) in both matrices $N(\gamma\gamma 2\alpha)/N(\gamma\gamma{}^{8}\mathrm{Be})$ is ≈ 4 and for ^{21}Ne (ground-state transition) this ratio is only ≈ 1.5. The total ratio of events $N(\gamma\gamma 2\alpha)/N(\gamma\gamma{}^{8}\mathrm{Be}) \approx 1.5$. The appearance of peaks due to transitions which belong to ^{23}Na in the "^{8}Be" gate (see fig. 13) cannot be attributed to two α's or ^{8}Be emission. This effect is due to lithium emission [14], overlapping with the ^{8}Be particle (ΔE-E) gate. This effect occurs only in the $^{18}\mathrm{O} + {}^{13}\mathrm{C}$ reaction, where the neutron excess gives more favourable Q-values for lithium emission than for the other reaction.

Using particle-γ coincidences, it was possible to investigate the energy dependence of the relative population

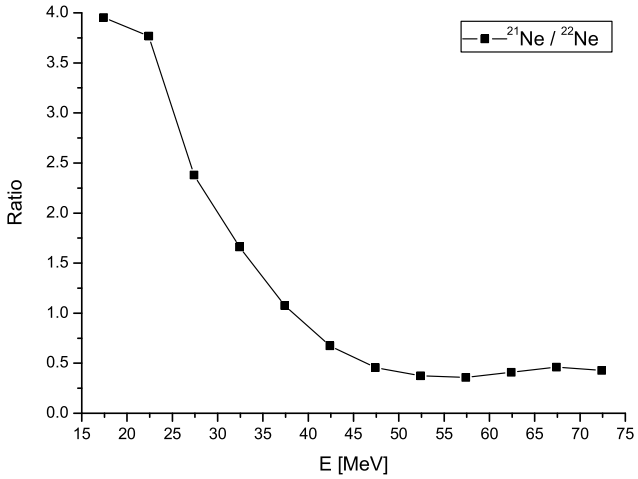

Fig. 15. Ratio between the populations of the transition from the first excited states in ^{21}Ne (350 keV) and ^{22}Ne (1274 keV) for different energies, E (*i.e.* the energies from the thick E detectors of ISIS), of the coincident two α-particles detected in the same detector (*i.e.* ^{8}Be).

of these nuclei by gating on different energies within the "^{8}Be" banana (see fig. 14). One can see that ^{8}Be is stronger by a factor of $2 \rightarrow 2.5$ than lithium. (Note that ^{23}Na already represents a subsequent $1n$ or $2n$ emission following the ejection of a ^{7}Li or ^{6}Li, respectively.)

As can be seen from fig. 15, ^{8}Be events are concentrated in the low-energy region of the $E_{\rm sum}$ distribution. This is in good agreement with the result shown in fig. 8, when plotting the ratio between the rates of the two α-particles registered in different detectors and in the same detector, as a function of the energy. The lower energies are enhanced, indicating ^{8}Be emission.

With the observation of various channels like two α, three α, ^{8}Be or ^{12}C*, a systematic dependence on the excitation energy in the residual nucleus in cluster emission can be found. Note that in the experimental systematics of Morgenstern *et al.* [15], the average energy carried by individual nucleons and α-particles is obtained as follows: i) each individual nucleon carries approximately 16.4 MeV (four nucleons, 66 MeV); ii) one α-particle carries approximately 22.3 MeV. Subtracting the α-particle binding energy of 24 MeV, the 4 nucleons should have carried away 42 MeV, much more than the 22.3 MeV of the four bound nucleons. In addition, the unequal energies carried by single protons and neutrons of 18.3 MeV and 13.2 MeV [15] respectively, point to the influence of the Coulomb barrier, $E_{\rm b}$.

We can consider the maxima of the energy spectra to be proportional to the Coulomb barrier in the centre-of-mass frame for the fragment-residual-nucleus system. With this assumption, it can be deduced that the maximum of the sum of the energies of the three α-particles is given (in MeV) by their Coulomb energies:

$$E_{3\alpha}^{\rm max} = \sum_{i=1}^{3} \left\{ \frac{1.44 \times Z_{i\alpha}(Z_{\rm CN} - Z_{i\alpha})}{R({\rm residue}, \alpha)} \right\} \qquad (23)$$

This value is larger than the maximum in the energy distribution of the emitted ^{12}C$^{*}(0_2^+)$ fragment, which can be determined by the expression (Coulomb energy)

$$E_{^{12}{\rm C}}^{\rm max} = \frac{1.44 \times 6(Z_{\rm CN} - 6)}{R(^{40}{\rm Ca}, ^{12}{\rm C})}\,, \qquad (24)$$

where the barrier radii are given by $R(A_1, A_2)(= R_0(\sqrt[3]{A_1} + \sqrt[3]{A_2})$, with $R_0 = 1.4$ fm). Considering the barrier energies in the centre-of-mass system in eqs. (23) and (24), the difference is 18%, giving a lower value for the ^{12}C cluster emission ($E_{^{12}{\rm C}}^{\rm max} = 21.6$ MeV and $E_{3\alpha}^{\rm max} = 26.5$ MeV). This points to the direction of the observed lower total energy carried by the ^{12}C* cluster. Note that there is no Q-value difference between the two cases. It is interesting to consider the ^{12}C$^{*}(0_2^+)$ state as a Bose-Einstein condensate with a r.m.s. radius of 4.29 fm, as calculated by Tohsaki *et al.* [16]. This further reduces the Coulomb barrier to 19.1 MeV. Likewise, the $E_{\rm b}$ for ^{8}Be and two α-particles, for example, differs by 1.5 MeV (lower for ^{8}Be). However, what one can see from the data is an even larger effect (see figs. 8 and 9): in both cases the maxima of the cluster emission energy spectra are shifted to lower energies (≈ 3 MeV for ^{8}Be and 14 MeV for ^{12}C$^{*}(0_2^+)$). The difference arising from the variation of the energies due to the kinematics (the Jacobians) (see figs. 3 and 4) is, however, too small. Possible explanations of this observation are given below.

3.4 The statistical decay process

We use the standard formulation of statistical decay [17] for the energy spectra of evaporated particles. The probability of emitting an α-particle in the energy range $\in \rightarrow \in + d \in$ from a nucleus with initial spin, I, in one evaporation process is given by the following equation:

$$P_\alpha(\in, I) d \in = \sum_{l=0}^{\infty} T_{l_\alpha}(\in) \sum_{J=|I-l|}^{I+l} \rho(E, J) d \in\,. \qquad (25)$$

Here, J and E are the spin and energy of the residual nucleus after the emission, respectively. The transmission coefficients, $T_{l_\alpha}(\in)$, are for the formation of the compound nucleus with the l-th partial wave of the incident particle. The spin-dependent level density can be expressed by [18]

$$\rho(E, J) = \sqrt{a} \sqrt{\left(\frac{\hbar^2}{2\Im}\right)^3} \frac{(2J+1)}{12(E - \Delta - E_{\rm rot})^2} \times e^{2a\sqrt{(E-\Delta-E_{\rm rot})}}\,. \qquad (26)$$

Here, $E_{\rm rot}$ is the rotational energy, Δ is the pairing energy and a is the level density parameter. The effective moment of inertia is $\Im$. For the total (energy-integrated) probability in the sequential process we have mainly a product of probabilities:

$$P_{n\alpha} \propto \prod_{i=1}^{n} \left(e^{\sqrt{E_i}}\right), \qquad (27)$$

where E_i is the excitation energy of the residual nucleus at each step of the decay process ($E_i = E_{i-1} - \in_i$, $E_0 = E_{\rm CN}$) and $\in_i$ are the energies of the sequentially emitted α-particles. Similarly, in the case of cluster emission, the probability is simply proportional to

$$P_{\rm cluster} \propto e^{\sqrt{E_{\rm RC}}}, \tag{28}$$

where $E_{\rm RC}$ is the excitation energy of the residual nucleus after cluster emission ($E_{\rm RC} = E_{\rm CN} - E_{\rm cluster}$) and $E_{\rm cluster}$ is the kinetic energy of the cluster, assumed to be

$$E_{\rm cluster} = \sum_i \in_i , \tag{29}$$

in order to isolate the level density effect.

One of the clearest features of the sequential emission is the fact that the level density enters into *each* single step of the sequential decay process, implying that the decay phase space enters several times. Therefore, the sequential decay will dominate over the cluster decay, but the observation that cluster decay leaves the residual nucleus with more excitation energy increases its likelihood.

However, special effects like strong deformation or clustering in the parent nucleus may enhance the emission of larger fragments, influencing the transmission factors. The transmission factors for the different fragments are usually obtained by the optical potential in the time-reversed exit channel. The spectra have an exponential shape, which is truncated at lower energies due to the Coulomb barrier (see sect. 3.3). In this case the lower Coulomb energy and the changed level density at scission could add up to the observed large difference in the total energy of the emitted binary fragment relative to the sequential α emission.

Other factors (in addition to the Coulomb barrier) that may shift the energies of the ^{12}C* to still lower energies are:

i) the dependence of the level density on the mass of the residual nucleus, but, more likely

ii) a significant effect is expected for the ^{12}C* if it is emitted from a deformed state. In the case of ^{12}C$^*(0_2^+)$ the large radial extension of the excited state [16], considered to be a Bose-Einstein condensate, further decreases the Coulomb-barrier energy (as shown in sect. 3.3).

Another important feature of the chosen reaction channels is the selective population of states with natural parity in the residual nucleus, if only particles with spin zero, like α-particles, ^{8}Be and ^{12}C* fragments, are emitted (see discussion on ^{40}Ca parity doublets in ref. [10]).

4 Summary and conclusions

In the present work with the use of a γ-detector ball in combination with a charged-particle detector ball, it was possible to study the emission of ^{8}Be and ^{12}C* clusters in compound nuclear reactions and to deduce the relative energies of the decay processes by analysing the coincident γ-spectra. The detection of the unbound cluster threshold states was possible by the detection of pile-up events in the ΔE-E telescopes of the ISIS array. Although these events appear along the same event line as the multiple-hit events, it was found that the double- and triple-hit events from multiplicities $M = 2$ and $M = 3$, respectively, give only a very small contribution to the ^{8}Be and ^{12}C* emission. The latter must be explained by the strong correlations of the sequentially emitted α-particles, which only in rare cases are emitted statistically independent in the emission cascade. The observed strong correlation in the two α particles, registered in different detectors ($F = 2$), can be most plausibly explained by ^{8}Be$^*(2^+)$ emission.

The cluster fragments, ^{8}Be *or* ^{12}C**, on average carry away less energy from the compound nucleus than two or three sequentially emitted α-particles.* In the case of cluster emission, corresponding to the same total (A, Z), the emission of another light (charged) particle from the residual nucleus is possible. The observed higher probability of sequential α-particle emission than of cluster emission is in agreement with expectations from the statistical model. These events populate states in the compound nucleus closer to the yrast line than the binary cluster emission process, because in the sequential process the level densities (which appear several times in the emission phase space) emphasise the emission of a higher total energy for the α-particles.

The method described here to observe ^{8}Be and ^{12}C* clusters lends itself as a special tool to detect states in excited nuclei with strong α correlations, *i.e.* Bose-Einstein condensates in nuclei.

This work was supported by the BMBF grant Nr. 06-OB-900 and the EU-LSF program (contract Nr. HPRI-CT-1999-00083). Dr H.G. Bohlen is thanked for commenting on the manuscript. Tz. Kokalova would like to thank the DAAD and A. Tumino and G. de Angelis the A.v. Humboldt foundation for their support.

References

1. S.J. Sanders, A. Szanto de Toledo, C. Beck, Phys. Rep. **311**, 487 (1999).
2. J. Gómez del Campo *et al.*, Phys. Rev. C **57**, 457 (1998).
3. E. Farnea *et al.*, LNL-INFN (Rep) **160/00**, 20 (2000).
4. S. Thummerer, B. Gebauer, H.G. Bohlen, W. von Oertzen, D. Bazzacco, S.M. Lenzi, A. Algora, G. de Angelis, A. Gadea, D.R. Napoli, C. Borcan, F. Dönau, L. Käubler, H. Schnare, R. Schwengner, I. Peter, C. Beck, C. Bhattacharya, M. Rousseau, R. Nouicer, J. Lisle, Phys. Scr. T **88**, 114 (2000).
5. E. Farnea, G. de Angelis, M. de Poli, D. De Acuna, A. Gadea, D.R. Napoli, P. Spolaore, A. Buscemi, R. Zanon, R. Isocrate, D. Bazzacco, C. Rossi Alvarez, P. Pavan, A.M. Bizzeti-Sona, P.G. Bizzeti, Nucl. Instrum. Methods Phys. Res. A **400**, 87 (1997).
6. D.P. Stahel, G.J. Wozniak, M.S. Zisman, B.D. Jeltema, J. Cerny, Phys. Rev. C **16**, 1456 (1977).
7. G.F. Knoll, *Radiation Detection and Measurement* (John Wiley and Sons Inc., New York, 1999).
8. E. Farnea, PhD Thesis, University of Surrey, Guildford, UK (2001).

9. S.Y. Van der Werf, Nucl. Instrum. Methods Phys. Res. A **153**, 221 (1978).
10. S. Torilov, S. Thummerer, W. von Oertzen, Tz. Kokalova, G. de Angelis, H.G. Bohlen, A. Tumino, M. Axiotis, E. Farnea, N. Marginean, T. Martinez, D.R. Napoli, M. De Poli, S.M. Lenzi, C. Ur, M. Rousseau, P. Papka, Eur. Phys. J. A **19**, 307 (2004).
11. S. Thummerer, W. von Oertzen, B. Gebauer, S. Lenzi, A. Gadea, D.R. Napoli, C. Beck, M. Rousseau, J. Phys. G **27**, 1405 (2001).
12. S. Thummerer, PhD Thesis, Freie Universität, Berlin, Germany (1999).
13. W. von Oertzen, Phys. Scr. **T88**, 83 (2000).
14. Tz. Kokalova, PhD Thesis, Freie Universität, Berlin, Germany (2003).
15. H. Morgenstern, W. Bohne, K. Grabisch, H. Lehr, W. Stoffler, Z. Phys. A **313**, 39 (1983).
16. A. Tohsaki, H. Horiuchi, P. Schuck, G. Röpke, Phys. Rev. Lett. **87**, 192501 (2001).
17. M. Blann, Phys. Rev. **157**, 860 (1967).
18. M. Rousseau, PhD Thesis, Université Louis Pasteur, Strasbourg, France (2002).